Assessment of the Required Maximum-Power-Point-Tracking Speed for Vehicle-Integrated Photovoltaics Based on Transient Irradiation Measurements and Dynamic Electrical Modeling

Leon Salomon,* Gustav Wetzel, Jan Krügener,* and Robby Peibst

Fast changing irradiation on vehicle-integrated photovoltaic (VIPV) modules may impose demanding requirements for maximum power point tracking (MPPT) to ensure high energy conversion efficiency. In this work, the results of simulations regarding the output and efficiency of an exemplary VIPV module under real-life irradiation conditions as measured with high time resolution are resulted. Herein, resistive as well as voltage source load is used as two idealized models of the MPPT. The simulations show that, in most cases, tracking with a resistive load at 1 Hz preserves above 90%$_{rel}$ of the convertible energy determined by the cell performances under given irradiance levels. With a voltage source load, these values do not undercut 97%$_{rel}$ at 0.1 Hz. Herein, it is also found that partial shading across the exemplary series connected module can reduce the converted energy in the range of 5–10%$_{rel}$ in relation to complete negligence of this effect.

1. Introduction

The transportation sector is one of the largest emitters of carbon equivalent and has not reduced its annual emission substantially within the past 30 years.[1] The ongoing electrification of vehicles is one way to tackle this issue, especially in combination with photovoltaics as a low-carbon-emitting electrical energy conversion.[2] As a specific application of this combination, vehicle-integrated photovoltaics (VIPV) can elongate the range of electric vehicles[3] and thus reduce stationary charging demands as well as take stress off the electric grid.[4] This said, VIPV faces some quite different conditions and challenges in comparison to stationary photovoltaic modules, which have been tackled by scientific research. For example, energy yield potential,[3,5,6] self-shading due to curved car surfaces,[7,8] and also dynamic irradiance conditions[9] have been investigated on different levels of measurements and modeling. Further elaborating the latter, shading of a VIPV module by objects, i.e., buildings, trees, street signs, or alike, is not only determined by the sun's position but also by the movement of the vehicle, changes can occur on a quite small timescale as examined in our previous work.[10] This results in correspondingly fast changes of the momentary maximum power point (MPP) of the solar panels and thus may impose high demands on a MPP tracking (MPPT) system, which should ensure high energy yield. On one hand, good performance in this regard is especially critical considering the limited space on a vehicle body; on the other hand, unnecessary system complexity and energy consumption due to data sampling should ideally be avoided. In this work, we investigate the effects of the transient and moreover partial shading on the energy conversion efficiency of an exemplary VIPV module and the arising demands on a MPPT system concerning tracking frequency. This is done by simulations with LTspice and high-frequency measurements of the irradiation onto a vehicle in exemplary real-life driving conditions. Existing literature is rather sparse regarding this kind of simulation of vehicle adjacent photovoltaic MPPT systems with measured irradiance profiles. Schuss et al.[11,12] combined real-life measurements and MPPT simulation as well but did not focus on the tracking and instead on the data sampling frequency of the measurement[11] or kept the investigated data samples rather limited, namely below 1 min.[12] Otherwise there is, to the best of our knowledge, no other publication to date featuring MPPT simulations and real-life measurements.

L. Salomon, G. Wetzel, J. Krügener, R. Peibst
Institute of Electronic Materials and Devices
Leibniz University Hannover
Schneiderberg 32, 30167 Hannover, Germany
E-mail: salomon@mbe.uni-hannover.de;
kruegener@mbe.uni-hannover.de

R. Peibst
Institute for Solar Energy Research in Hamelin
Am Ohrberg 1, 31860 Emmerthal, Germany

The ORCID identification number(s) for the author(s) of this article can be found under https://doi.org/10.1002/solr.202300795.

2. Irradiation Measurements

The measurements of the irradiation were performed using three silicon-type pyranometers mounted on the roof of a

Table 1. Specifications of the conducted test runs for measurement of partial shading.[a]

Season	Winter	Summer	Autumn
Date	28.02.2020	24.06.2020	05.11.2020
Time (UTC)	11:53–12:41	7:56–8:36	09:38–10:16
Solar zenith angle[20]	29.5–27.91°	41.34–47.03°	19.27–20.98°
Solar azimuth angle[20]	185.5–198.93°	105.93–115.98°	157.91–167.47°
Mean global radiation[21]	397 W m^{-2}	837 W m^{-2}	353 W m^{-2}
Mean diffuse radiation[21]	197 W m^{-2}	73 W m^{-2}	73 W m^{-2}

[a]The radiation values were measured stationary and closely located to the test route by the Institute of Meteorology and Climatology, Leibniz University Hannover.

passenger car with a sampling frequency of 1000 Hz. All measurements were carried out on a circular test route in Hannover, Germany, of approximately 20 km length consisting of slowly driven narrow streets, fast driven wide streets, and slowly driven wide streets. Further specifications as well as more details to setup and data acquisition are given in our previous work.[10] In this work, we perform simulations with values acquired by two types of measurement configurations as input: first and mainly with all three pyranometers pointing upward and placed in line with driving direction and approximately 60 cm distance in between to acquire information about partial shading; second with one pyranometer pointing upward and the remaining two pointing to the sides as described in our previous work.[10]

In the partial shading configuration, three test runs under sunny conditions were conducted with the specifications shown in **Table 1**. The clear weather condition was on one hand observed with a vehicle-mounted camera and is on the other hand further illustrated by the fact that the stationarily measured global irradiance is significantly exceeding the diffuse irradiance. The test runs in the roof-side configuration are the ones specified and analyzed in our previous work.[10]

3. Simulation Model

The simulated module consists of 35 cells connected in series and arranged in a 7×5 array as depicted in **Figure 1**a. Resistances for cell and series interconnecting ribbons were inserted between every cell and substring respectively (see Table S1, Supporting Information).[13] Bypass diodes, in contrast, were not implemented into the module. The model of the single solar cells is based on two-diode parameters (see Table S2, Supporting Information) of measured (2 × 2) cm^2 polysilicon on oxide (POLO) solar cells with interdigitated back contacts (IBCs). This specific cell architecture exhibits a considerably high efficiency potential of well above 25%,[14] which is important given the confined area on a vehicle. Furthermore, the use of IBC is especially suitable for vehicle integration since a relatively even optical appearance can be achieved and losses by reflection on front-side metallization are prevented. These cells were scaled up to M2 size to resemble cells used in an exemplary VIPV module, which results in the specific simulated cell parameters depicted in **Table 2**.

Furthermore, two parallel capacitances are employed in every cell model to give credit to the transient characteristic of the cell output. This was measured with the setup described in our previous work[15] and showed similar behavior as the cells examined therein. The observed decay times of the POLO cells investigated in this article range from few 10 to few 100 μs depending on the connected Ohmic load and resulting steady-state cell voltage. Although these measured values are smaller than even the sample frequency, transient times may become relevant for

Table 2. Parameters of the modeled M2-sized POLO solar cells as given by simulation.

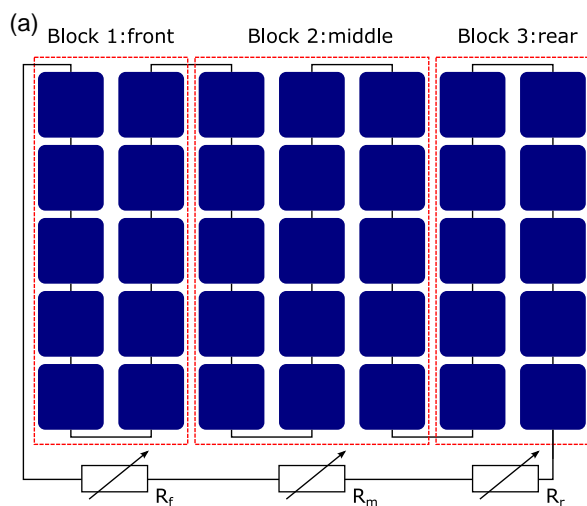| Quantity	J_{sc}	V_{oc}	η_{STC}	FF
Unit	[mA cm^{-2}]	[mV]	%	[%]
Value	39.58	702	22.52	80.81

Figure 1. Simulation and measurement setups. a) Schematic drawing of the simulated solar module with resistive MPPT load. b) Photography of the used pyranometer setup for high frequency measurements of irradiance.

module performance when multiple larger cells are circuited and interconnection resistances are present.

So the first of the mentioned capacitances is a diffusion capacitance C_{diff}, holding the voltage-dependent charge

$$Q = A \cdot d \cdot \Delta n(V) \tag{1}$$

with the cell area A, cell thickness d, and the excess carrier density $\Delta n(V)$ as described in one of our previous works.[15] The second capacitance is the depletion capacitance C_{dep}. C_{diff} was modeled using the referenced equations with parameters of the examined cells (see Table S3, Supporting Information), while, in relation, only weakly voltage-dependent C_{dep} was assumed as constantly $1\,\mu F\,cm^{-2}$ to fit the observed behavior.

It is worth mentioning that the POLO–IBC cells characterized and simulated here pose an intermediate status of our cell development. Although they do not exploit the full efficiency potential of this structure, they are sufficiently representative for the aspects investigated in this work. In particular, higher effective lifetimes and thus higher open-circuit voltages up to 720 mV are now achieved by mitigating recombination losses.[16] Additionally, the transient times of a circuited cell appear to be more sensitive to the connected load than its capacitances. This was tested experimentally for different cells with the setup described in our previous work[15] and confirmed with the simulations of this publication. An explanation for this behavior may be that in a circuited case $\Delta n(V)$ is mainly affected by the flow of charge carriers through the load and not by the carrier lifetime, which is a cell inherent property.

Regarding the module simulation, measured irradiation was considered as linearly scaled photocurrent values I_{ph} as input to every single cell. This behavior of I_{ph} was confirmed by measurements with a solar simulator (see Figure S1, Supporting Information). As an overview of the simulated weak-light performance of the cells, we also included current density–voltage and efficiency–voltage characteristics in dependence of S, Figure S2, Supporting Information. To give credit to inhomogeneous irradiation across the module area due to shading by passing structures, the modules were divided into three homogeneously irradiated domains. The respective input values originate from irradiation measured by pyranometers mounted on the front, middle, and rear of the roof of the test vehicle as shown in Figure 1b. To eliminate the effect of current mismatch induced by this partial shading as well as the resulting loss in conversion efficiency and thus evaluate the maximum achievable efficiency gain by bypass diodes, all simulations were also carried out with the different domains electrically separated into three independent circuits. An investigation of optimal device parameters of bypass diodes and circuiting would go beyond the constraints of this publication.

The MPPT load, in a partial shading case one independently controlled for and by every irradiation domain as shown in Figure 1a, was simulated in two idealized ways: first as an adjustable Ohmic resistance and second as an adjustable voltage source, which both represent two important types of loads on a photovoltaic module.[17] In both cases, the load value (R_{MPP} or V_{MPP}), which ensures operation of one solar cell at its MPP, was simulated in dependence of the irradiance S as depicted in **Figure 2**. As mentioned before, it was assumed that S scales I_{ph} of the cells
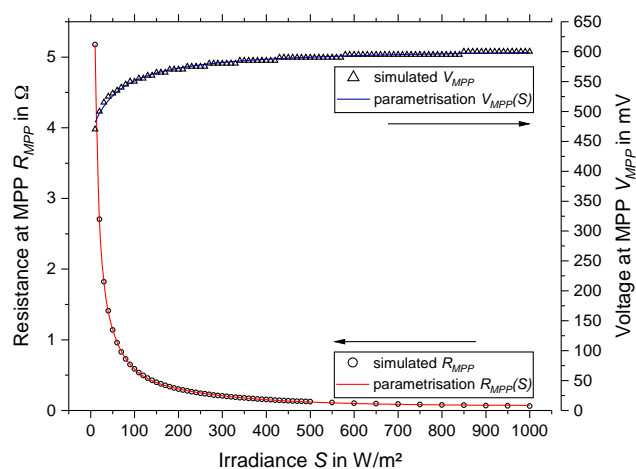

Figure 2. Simulated values of the resistance and voltage at the MPP R_{MPP} and V_{MPP} in dependence of the irradiance S and the used fitting functions.

linearly. The respective values $R_{MPP}(S)$ and $V_{MPP}(S)$ were then fitted with parameterizations, which was used as the function to control the respective load directly by S. It can be seen in both cases that the dependency is especially strong for irradiance below $200\,W\,m^{-2}$ and generally weaker for the voltage source. Hence, mainly low irradiance and changes into this region may be limiting the tracking effectiveness.

Different tracking frequencies f_{MPPT} were simulated by keeping the respective load constant for a time interval $T_{MPPT} = 1/f_{MPPT}$ and readjusting it instantly to the value assigned to the momentary irradiance.

4. Results and Discussion

All following results are based on the simulated converted energy E_{conv} of the explained module for a given test run and street type. All shown efficiency values are based on the cumulated cell area only with the assumption of a fixed cell temperature of 25 °C. All depicted error bars ($k = 1$) originate from different energy yields for five different simulated tracking starts randomized within a tracking period in addition to a tracking start exactly with the start of the part of the test run. In general, these deviations decrease steeply with increasing f_{MPPT} and are nearly irrelevant above 1 Hz, but quite significant below showing values of up to $2\%_{abs}$ equating $15\%_{rel}$.

To give a brief estimation of the energy conversion potential of the used exemplary VIPV modules (with $\approx 192\,W_p$), the maximum converted energy (assuming perfect tracking) for each test drive and street type is shown in **Table 3**.

Table 3. Maximum converted energy of one simulated VIPV-module with 7×5 M2 cells ($\approx 192\,W_p$) assuming perfect tracking in kWh.

	Narrow Slow	Wide Fast	Wide Slow	Whole Test Drive
Winter	0.0073	0.0023	0.0201	0.0296
Summer	0.0153	0.0102	0.0348	0.0601
Autumn	0.0045	0.0038	0.0109	0.0192

For context, Peibst et al. identified an energy demand of roughly 4 kWh per 20 km, which is approximately the length of test route in this work, for an exemplary utility vehicle, on whose roof five of the simulated modules can be integrated.[14] With the assumption of equal energy conversion by all five hypothetical modules our simulation gives, i.e., of the summer drive, roughly 7.5% solar coverage of the needed driving energy at best, namely assuming, later explained, perfect tracking, and not considering further transfer losses in the vehicle's energy system. This coincides quite well with the results from Peibst et al.,[14] who found approximately 12% solar coverage during 30 km test drive on a late spring day (May 31, 2021, 8:45 UTC), but with additional consideration of solar modules on the vehicle sides and back.

4.1. Resistive Load

Figure 3 shows the mean efficiencies (arithmetic mean over driving time for each street type) of the energy conversion $\overline{\eta}$ by one module calculated in dependence of the simulated tracking frequency f_{MPPT} for partial shading, grouped in street type and season. The general tendencies are similar in all cases with $\overline{\eta}$ converging to the maximum value at 1000 Hz, which is to our knowledge not technically achievable and accounted for as "perfect tracking" (within the framework of the model). This value depends significantly on the overall performance of the solar cells and thus on the mean irradiance, which is exhibited in the differences among seasons. The gap between perfect tracking efficiency and η_{STC}, which is depicted as the dashed line, is in parts more than $2\%_{abs}$ and quite considerable. On a sidenote, this specific value does not solely originate from irradiation below STC level but rather from a combination of this and partial shading. This fact can be seen in comparison with the later shown graphs (see Figure 5) for simulations, in which partial-shading effects are completely neglected. The difference between perfect tracking and η_{STC} there is still well above $1\%_{abs}$.

One remarkable tendency seen in Figure 3 is also the generally weaker efficiency for fast driven wide streets at non-perfect tracking. This could be explained by the fact that shading is mainly caused by trees, which have relatively small feature sizes and thus exhibit fast changes in the irradiance values. Nonetheless, this trend is likely, and at least for the winter drive probably significantly, enhanced by the systematic occurrence of observable measurement noise on a specific part of the fast driven wide streets in all test runs, making up for roughly a quarter of the respective driving duration. Exemplary irradiation data as well as frequency analysis of the measurement noise can be found Figure S3 and S4, Supporting Information. However, to date, we found no explanation for the origin of this noise.

Relating all yields to the perfect tracking case, as illustrated in **Figure 4**, shows potentially large losses of well above $20\%_{rel}$ for $f_{MPPT} = 0.1\,Hz$. However, because of the steep increase in yield for these slow tracking speeds, only small losses of well below $5\%_{rel}$ can be stated for the simulated frequencies above 1 Hz. Thus, it may be reasonable to employ tracking at this value since any increased technical demand would be rewarded only by these relatively small gains.

Especially the maximum losses are in good agreement with the values simulated from Schuss et al.[12] for MPPT based on sampling of momentary V_{OC}[18] with irradiance values measured at 10 Hz.

Figure 5 shows the mean efficiencies with complete negligence of partial shading across the module. Nearly the same tendencies as in the partially shaded case can be observed in combination with overall higher-efficiency values. For example, the perfect tracking case in the summer would almost convert energy with STC efficiency (average irradiation $\gg 510\,W\,m^{-2}$). For winter and autumn, however, even perfect tracking results in efficiencies far below the STC values. One possible explanation could be the low average illumination intensities ($\approx 246\,W\,m^{-2}$ for winter and $\gg 179\,W\,m^{-2}$ for autumn). Within the framework of the two-diode model, a lower efficiency for lower illumination intensities can, in addition to the lower voltage in addition to the linearly decreased generation current density, also be expected from the stronger impact of the shunt resistance and the second diode with an ideality factor of 2 at lower voltages. Thus, the weak-light behavior of the solar cells might be more relevant for VIPV applications than for stationary applications with less shading and more favorable orientation of the modules toward
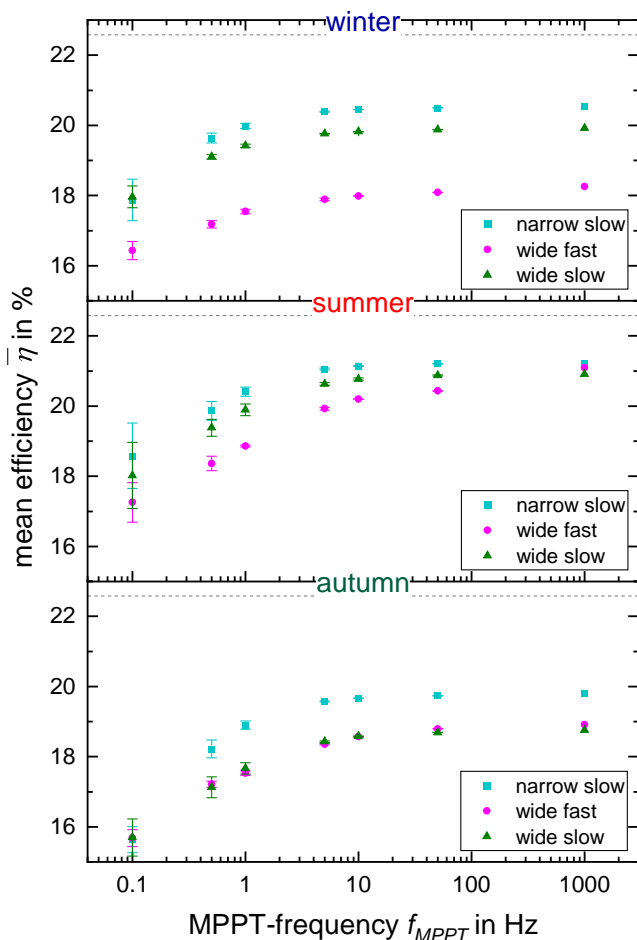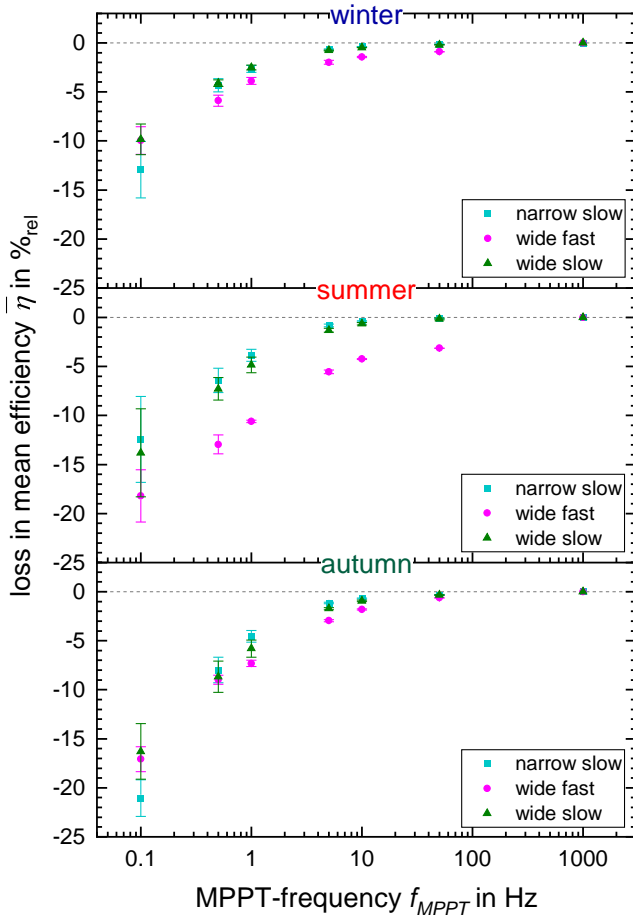

Figure 3. Simulated mean efficiencies for exemplary test drives in dependency of the tracking frequency of resistive load and the street type with consideration of partial shading.

ADVANCED
SCIENCE NEWS
www.advancedsciencenews.com

Solar
RRL
www.solar-rrl.com

Figure 4. Efficiency losses depending on the tracking frequency of a resistive load relative to tracking with 1000 Hz and consideration of partial shading.

Figure 5. Simulated mean efficiencies without partial shading losses for resistive load.

the sun. Consequently, an optimization of the weak-light behavior of the solar cells is desirable. The mentioned difference in conversion efficiency can explicitly be observed in **Figure 6**, where the relative losses due to partial shading normalized to the case without partial shading are shown. These losses range from 5 to 10%$_{rel}$ and show no systematic dependency of the tracking frequency. Thus, implementation of bypass diodes or usage of an alternative cell connection such as strings in parallel might be favorable to mitigate these losses.

4.2. Voltage Source Load

As mentioned before, all aforementioned simulations were also carried out with an ideal voltage source as the module's load. The conversion efficiencies for the perfect tracking case show slightly higher values in relation to the resistive load. The reason for this behavior is not known so far and needs further investigation. However, the losses due to not perfect tracking, as depicted in **Figure 7**, show a similarly converging trend as for the resistive case, but with much smaller values. Precisely, they are not exceeding 3%$_{rel}$ even for 0.1 Hz tracking frequency, which can
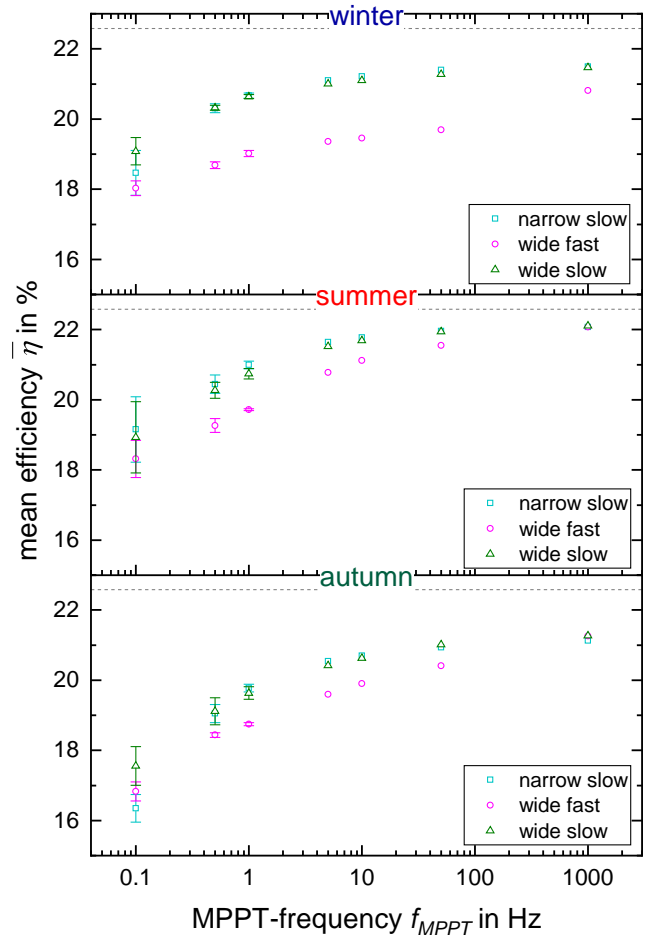
be traced back to the narrow range of V_{MPP} variation. This points strongly to implementing a voltage-type load, from which relatively low demands on the tracking frequency arise.

It has also to be noted that deviances in E_{conv} for randomized tracking starts are negligible; hence error bars are not shown.

4.3. Roof-Side Measurements Without Partial Shading

Lastly, simulations with irradiance values from roof-side measurements, which are described in detail in our previous work,[10] were performed. These simulations had to assume homogeneous irradiation on the given module because of the measurement with only one pyranometer for each direction. Analogously to the previous section, the converted energies by a perfectly tracked 7×5-cells module are shown in **Table 4**. It has to be noted again that partial shading effects are completely neglected in this calculation, thus the values are overestimations.

Since the tendencies for different street types are quite similar to the ones in the former section, the mean efficiency for the whole given test runs are shown in **Figure 8**, grouped in different seasons as well as sunny and cloudy conditions with resistive load.
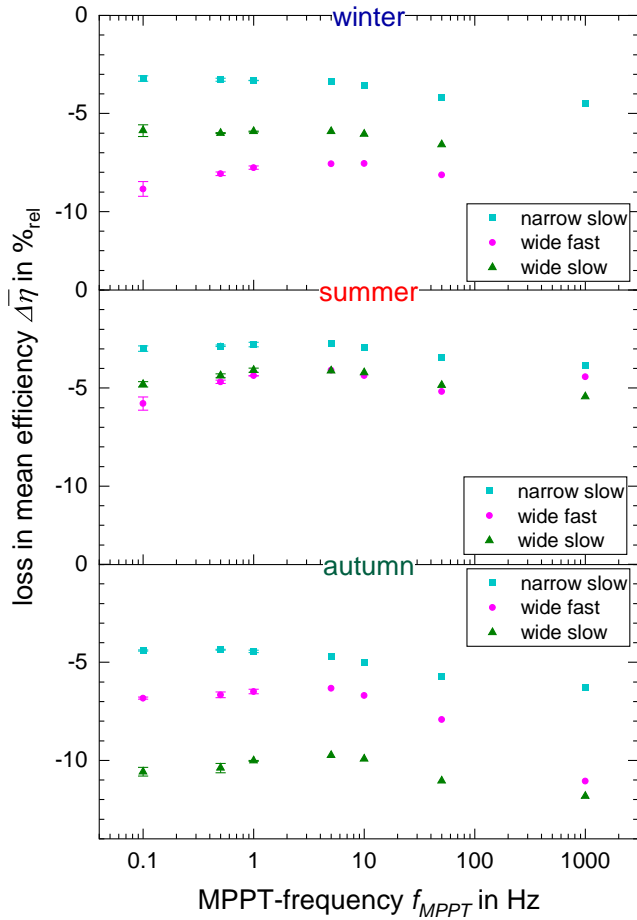
Figure 6. Relative loss due to partial shading over the simulated module for resistive load.

Figure 7. Simulated mean efficiency losses for voltage-source-based tracking. Closed symbols show losses by imperfect tracking, open symbols show losses by partial shading.

Table 4. Maximum converted energy of one simulated VIPV-module with 7 × 5 M2 cells ($\approx 192 W_p$) assuming perfect tracking in kWh during the respective test drive as specified in our previous work[a].[10]

		Left Side	Roof	Right Side
Autumn	Cloudy	0.0168	0.0434	0.0133
	Sunny	0.0182	0.0550	0.0199
Winter	Cloudy	0.0054	0.0139	0.0049
	Sunny	0.0178	0.0198	0.0107
Summer	Cloudy	0.0064	0.0153	0.0047
	Sunny	0.0312	0.0912	0.0194

[a]The weather conditions were observed by a car-mounted camera and verified by the difference between stationarily measured direct and diffuse irradiation as further described in our previous work.[10]

In general, higher efficiencies are present for roof irradiation with otherwise equal conditions, which originates from the better cell performance under the present higher irradiation. For the same reason, the efficiencies for sunny conditions are higher at perfect tracking as well as most high frequencies. With decreasing tracking frequency, the efficiencies under cloudy conditions decrease in a smaller fashion than under sunny conditions and thus show higher efficiencies for f_{MPPT} smaller than 1 Hz in most cases. This trend may originate from less variations of the irradiation with almost no direct solar irradiation present, leading to a smaller variation in the MPP resistance and thus less operation far away from the MPP. This translates into relative losses of below 10%rel even for tracking with 0.1 Hz and is an argument for lower tracking frequencies even with the lossier resistive load.

4.4. Possible Differences between Simulations and Real-World Systems

First, it has to be noted that the impact of the modeled transient behavior of the cells is neglectable under the measured irradiation changes as it could be expected by the small decay times of
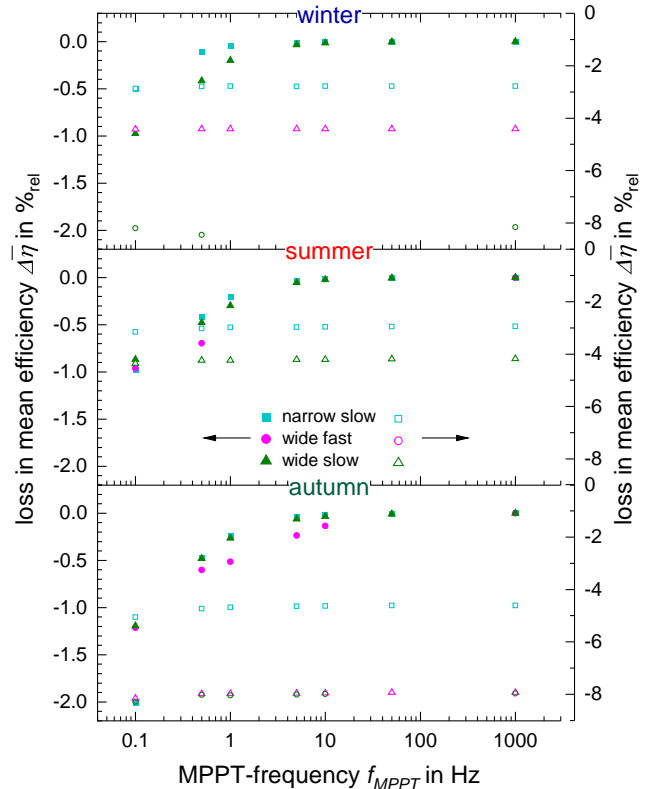
the cell output. Simulations with and without implementation of diffusion and depletion capacitance show only marginal differences in energy yield in the range of few 1%rel regardless of load. As illustration of the upper boundaries, the relative differences between simulations with and without both capacitances for the partially shaded 7 × 5 module with resistive load are shown in **Figure 9**. Solely on the wide driven fast streets, 1% of difference is surpassed, which is likely skewed by the measurement noise as discussed earlier.
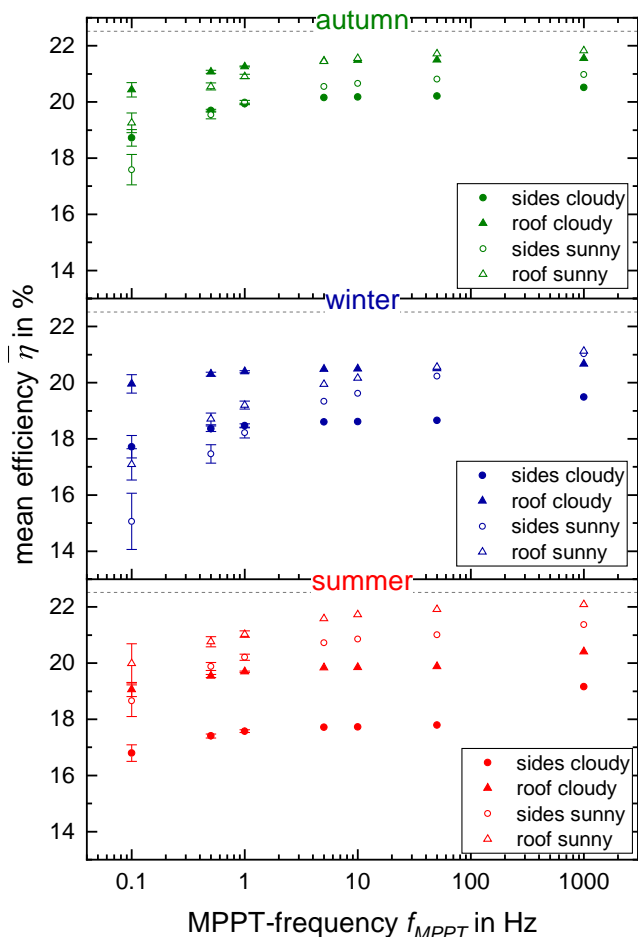
Figure 8. Simulated mean efficiencies for irradiation measured on the vehicle roof and sides under different weather conditions for resistive load.

Figure 9. Relative difference in energy yield $(E_{conv} - E_{conv,noC})/E_{conv}$ between simulations with and without implementation of cell capacitances for partially shaded module with resistive load.

Furthermore, limitations of our idealized model have to be considered in the interpretation of the shown results. In this regard, the instantaneous adjustment to the MPP is critical since it neglects two main factors of real tracking: 1) The specific MPP search algorithm, which can, especially for hill–climbing methods and under fast changing energy output conditions, even shift the working point away from the momentary MPP[18] and 2) The settlement time for tracking and setting the working point, which is in the range of 10 or even 100 ms.[19]

The influence of these factors will likely change the appearance of the shown graphs and trends. The consideration of a finite settlement time, i.e., reduces the time the system is working at the MPP in a given tracking cycle. This effect might be especially relevant for high frequencies, because the relative difference in this domain would be very high. This may shift the assessment to slower tracking frequencies.

On a wider scope, it has to be considered that the amount of driving time on the daily insolation time onto a vehicle is not unity and strongly dependent on its type. Namely, while this ratio might be quite high for long range transport, it may be only a small fraction in case of short range utility or passenger vehicles. So for the latter, even high losses during driving due to slow
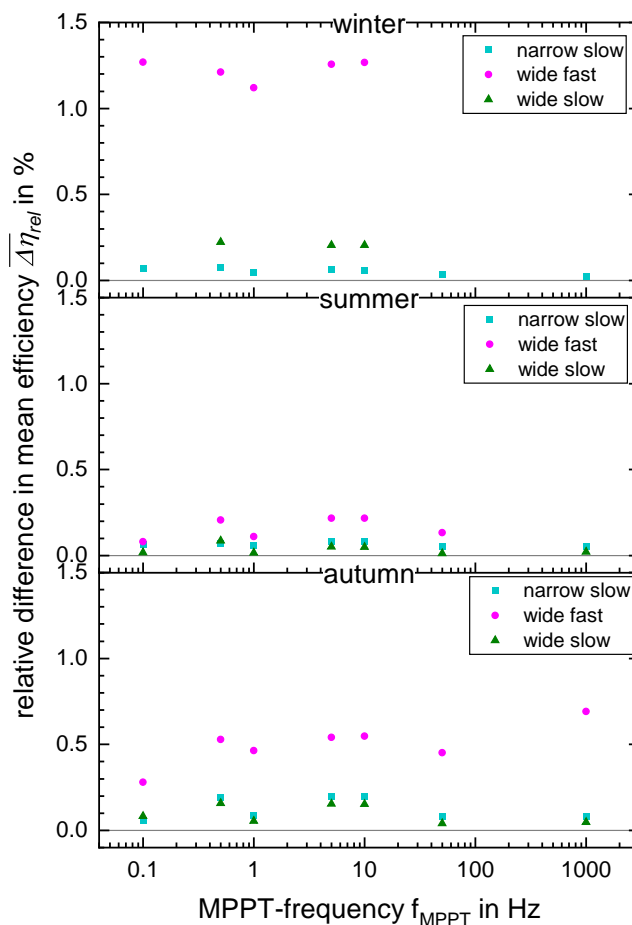
tracking might potentially be not as striking, when compared to the solar energy yield during a whole day and slower tracking frequencies can reasonably be implemented.

5. Conclusion

In this work, we simulated the output and efficiency of an exemplary VIPV module under real-life solar irradiation conditions while driving, which we measured on several test runs with a passenger car. Our simulations are based on the two-diode model of measured POLO silicon solar cells with consideration of transient behavior by cell capacitance and two idealized MPPT models, namely as adjustable resistance and voltage source respectively.

These simulations pointed on one hand toward a required tracking frequency of around 1 Hz for a resistive load, since frequencies below show considerable losses of up to 25%$_{rel}$ and above only small losses of mostly below 5%$_{rel}$ both in relation to hypothetical perfect tracking with 1000 Hz under sunny conditions. Cloudy conditions reduce the maximum losses to around 10%$_{rel}$.

On the other hand, a frequency of 0.1 Hz suffices to preserve above 95%$_{rel}$ of the convertible energy with an adjustable voltage source load even at high direct irradiation.

In both cases, the mentioned consideration of the transient behavior of the investigated solar cells leads only to insignificant differences of well below 1%$_{rel}$ in energy yield compared to completely neglecting it. Because of this weak influence of the cell capacitance itself both in transient times on cell level as well as overall energy yield, the results of the performed simulations will likely hold up for cells with even higher capacitances.

Lastly, partial shading due to passing structures accounts for losses of 5–10%$_{rel}$ regardless of the load type and tracking frequency on an exemplary module with one string of solar cells. Thus, implementation of another connection scheme like substrings in parallel or the use of bypass diodes is suggested.

Supporting Information

Supporting Information is available from the Wiley Online Library or from the author.

Conflict of Interest

The authors declare no conflict of interest.

Data Availability Statement

The data that support the findings of this study are available from the corresponding author upon reasonable request.

[1] European Environment Agency, *Greenhouse Gas Emissions from Transport in Europe* **2022**, https://www.eea.europa.eu/en/analysis/indicators/greenhouse-gas-emissions-from-transport (accessed: December 2022).

[2] M. J. de Wild-Scholten, *Sol. Energy Mater. Sol. Cells* **2013**, *119*, 296.

[3] R. Peibst, H. Fischer, M. Brunner, A. Schießl, S. Wöhe, R. Wecker, F. Haase, H. Schulte-Huxel, S. Blankemeyer, M. Köntges, C. Hollemann, R. Brendel, G. Wetzel, J. Krügener, H. Nonnenmacher, H. Mehlich, A. Salavei, K. Ding, A. Lambertz, B. Pieters, S. Janke, B. Stannowski, L. Korte, *Sol. RRL* **2022**, *6*, 2100516.

[4] K. Araki, A. J. Karr, F. Chabuel, B. Commault, R. Derks, K. Ding, T. Duiguo, N. J. Ekins-Daukes, J. Gaume, T. Hirota, O. Kanz, K. Komoto, B. K. Newman, R. Peibst, A. Reinders, *State-of-the-Art and Expected Benefits of PV-Powered Vehicles*, International Energy Agency - Photovoltaic Power Systems **2021**.

[5] M. C. Brito, T. Santos, F. Moura, D. Pera, J. Rocha, *Transp. Res. Part D Transp. Environ.* **2021**, *94*, 102810.

[6] M. Yamaguchi, K. Nakamura, R. Ozaki, N. Kojima, Y. Ohshita, T. Masuda, K. Okumura, A. Satou, T. Nakado, K. Yamada, T. Tanimoto, Y. Zushi, T. Takamoto, K. Araki, Y. Ota, K. Nishioka, *Sol. RRL* **2023**, *7*, 2200556.

[7] Y. Ota, T. Masuda, K. Araki, M. Yamaguchi, *Coatings* **2018**, *8*, 432.

[8] Y. Ota, K. Araki, A. Nagaoka, K. Nishioka, *Prog. Photovoltaics Res. Appl.* **2022**, *30*, 152.

[9] K. Araki, Y. Ota, M. Yamaguchi, *Appl. Sci.* **2020**, *10*, 872.

[10] G. Wetzel, L. Salomon, J. Krügener, D. Bredemeier, R. Peibst, *Prog. Photovoltaics Res. Appl.* **2022**, *30*, 543.

[11] C. Schuss, T. Fabritius, B. Eichberger, T. Rahkonen, *IEEE Trans. Instrum. Meas.* **2019**, *68*, 1485.

[12] C. Schuss, T. Kotikumpu, B. Eichberger, T. Rahkonen, in *20th IMEKO TC4 Inter. Symp. and 18th Int. Workshop on ADC Modelling and Testing*, Benevento, Italy.

[13] R. Witteck, *Doctoral Thesis*, Leibniz University Hannover, Hannover **2019**.

[14] R. Peibst, F. Haase, B. Min, C. Hollemann, T. Brendemühl, K. Bothe, R. Brendel, *Prog. Photovoltaics Res. Appl.* **2022**, *31*, 327.

[15] G. Wetzel, J. Krügener, B. Stannowski, S. Janke, R. Peibst, in *SiliconPV 2021, The 11th Int. Conf. on Crystalline Silicon Photovoltaics*, AIP Conference Proceedings, AIP Publishing, Hamelin, Germany **2022**, p. 030014.

[16] F. Haase, C. Hollemann, N. Wehmeier, K. Bothe, B. Min, H. Schulte-Huxel, R. Brendel, R. Peibst, *Sol. RRL* **2022**, *6*, 2200583.

[17] D. Shmilovitz, *IEE Proc. Electr. Power Appl.* **2005**, *152*, 239.

[18] T. Esram, P. L. Chapman, *IEEE Trans. Energy Convers.* **2007**, *22*, 439.

[19] Y. Levron, D. Shmilovitz, *IEEE Trans. Circuits Syst. I Regul. Pap.* **2013**, *60*, 724.

[20] T. Hoffmann, https://www.suncalc.org/#/52.3896,9.7168,3 (accessed: December 2022).

[21] Institute of Meteorology and Climatology, Leibniz University Hannover, https://www1.muk.uni-hannover.de/hp-design2020/weather_archive_frame_en.html (accessed: December 2022).